Available online at www.sciencedirect.com
ScienceDirect
C. R. Physique 10 (2009) 560–574
COMPTES RENDUS PHYSIQUE

Theoretical spectroscopy / Spectroscopie théorique

Theory of dielectric screening and electron energy loss spectroscopy at surfaces

Conor Hogan *, Maurizia Palummo, Rodolfo Del Sole

European Theoretical Spectroscopy Facility (ETSF), CNR-INFM-SMC, and Department of Physics, University of Rome "Tor Vergata", Via Della Ricerca Scientifica 1, 00133 Rome, Italy

Available online 25 April 2009

Abstract

We present an overview of theoretical techniques for describing electron energy loss processes in a reflection geometry. We start from a fundamental representation of the dielectric susceptibility tensor of the semi-infinite crystal, and illustrate how the screening becomes modified by the presence of the surface. A new formalism is also presented which improves upon existing techniques for modeling energy loss, is fully **q**-dependent, and accounts for nonlocality. The impact of nonlocality, local field effects and other many-body effects is discussed. The theory is supported by some explicit calculations on the GaAs(001)–$c(4 \times 4)$ surface. ***To cite this article: C. Hogan et al., C. R. Physique 10 (2009).***
© 2009 Académie des sciences. Published by Elsevier Masson SAS. All rights reserved.

Résumé

Théorie de l'écrantage diélectrique et de la spectroscopie de perte d'énergie pour une surface. Nous présentons une vue d'ensemble des techniques théoriques pour la description des processus de perte d'énergie des électrons dans une géométrie de réflexion. Nous partons d'une représentation fondamentale du tenseur de susceptibilité diélectrique du cristal semi-infini, et nous montrons comment l'écrantage est modifié par la présence de la surface. Nous présentons aussi un nouveau formalisme qui améliore les techniques existantes de modélisation des pertes d'énergie, prend pleinement en compte la dépendance en **q**, et la non-localité. L'impact de la non-localité, des effets de champs locaux et d'autres effets à plusieurs corps est discuté. La théorie est illustrée par des calculs explicites pour la surface GaAs(001)–$c(4 \times 4)$. ***Pour citer cet article : C. Hogan et al., C. R. Physique 10 (2009).***
© 2009 Académie des sciences. Published by Elsevier Masson SAS. All rights reserved.

Keywords: EELS; HREELS; Local field effects; Surfaces

Mots-clés : EELS ; HREELS ; Effets de champs locaux ; Surfaces

1. Introduction to HREELS

Electron energy loss spectroscopy (EELS) has proven to be an excellent technique for material characterization due to its versatility. The domain of application extends across a huge variety of phenomena, ranging from surface

* Corresponding author.
E-mail addresses: conor.hogan@roma2.infn.it (C. Hogan), maurizia.palummo@roma2.infn.it (M. Palummo), rodolfo.delsole@roma2.infn.it (R. Del Sole).

1631-0705/$ – see front matter © 2009 Académie des sciences. Published by Elsevier Masson SAS. All rights reserved.
doi:10.1016/j.crhy.2009.03.015

vibrations of the order of meV right up to core level transitions above 1 keV. Correspondingly, EELS has been used for studying the full spectrum of materials, including bulk, surfaces and interfaces, and more recently, nanostructured materials [1].

The high resolution form of the technique, HREELS, is carried out in a reflection geometry using incident electron beams with kinetic energy in the range 1–10 eV. The potential of HREELS for studying surfaces became apparent following experimental studies of Si(111) and the ZnO surface by Ibach [2]. More recently, it has been extended to probe the surface anisotropy [3,4], in a manner similar to that achieved with light in the technique of reflectance anisotropy spectroscopy (RAS).

Experimentally it was observed that the inelastically scattered electrons are concentrated in a narrow cone around the specular direction. This indicates that the impinging electrons start to interact with the surface at a relatively long distance from it ($\approx$100 Å), and hence, over a long period of time. Such scattering is known as *dipolar scattering* since the electrons interact with the long-range dipole field of the elementary excitations of the solid. Other regimes of scattering do exist, including *impact scattering*, which is characterized by large angle scattering from short range atomic potentials [5]. Theoretical description of impact scattering is difficult, however, and although some attempts have been successful [6], in this work we will only consider the dipolar regime.

Several theoretical formulations of EELS in a reflection geometry have been developed. For a thorough review of the various approaches, we refer the reader to the literature [7]. The earliest semiclassical[1] theory is known as the *dielectric theory* and was proposed by Lucas and Šunjić [8]. Being semiclassical it does not account for some important quantum mechanical effects, such as the reflection coefficient, and hence a quantum mechanical theory was subsequently developed by Mills [9]. Nevertheless, the use of the dielectric theory can be justified by the experimental conditions, and furthermore was *a posteriori* justified by the successful interpretation of measured spectra—for instance, Ibach's measurements on ZnO [2]. In this work we will consider inelastic electron scattering within a modified context of this semiclassical picture.

In the original formulation of the theory, an ideal surface was considered, i.e., a semi-infinite continuum having a constant dielectric function right up to the surface [8]. In reality, of course, the dielectric properties of a material change dramatically close to the surface due to the breaking of local symmetry, surface relaxation, formation of reconstructions, and so on. An improved description of the real surface is to consider a three-layer system, comprising vacuum, a surface layer and the underlying bulk [10,11].

This picture was further extended by Selloni and Del Sole [12] to account for anisotropy in the surface layer, in an approach which was also valid in the case of large momentum transfer parallel to the surface. Esquivel-Sirvent and Noguez [13] modified this approach to include anisotropy in the bulk layers (i.e., dichroism). The latter theories constitute the state of the art for describing electron energy loss at surfaces in the dipolar regime, and have been used with success on several systems [14,15]. Similar expressions have been developed for describing inelastic scattering from nanoparticles [16]. Of course, the use of a three-layer model to represent the semi-infinite crystal has not been restricted to energy loss; rather, it has been applied for years to interpret photon spectroscopies including RAS [17] and surface differential reflectivity [18]. It has been shown that the three-layer model is equivalent to the quantum mechanical theory of surface optical properties at normal incidence, provided that the surface layer dielectric function is suitably chosen. Nevertheless the validity of the approach for HREELS, where the penetration in the solid is less than that of light, is *a priori* questionable.

In this article we return to the problem of inelastic scattering of slow electrons at a surface, or, equivalently, the dielectric response of a surface to an external perturbation. We begin by introducing the mathematical quantities required to describe the process of electron energy loss at a surface. The subsequent section (Section 3) considers the dielectric susceptibility tensor appropriate for modeling EELS. How this tensor screens the perturbing charge in a semi-infinite system is dealt with in Section 4, which thus relates the microscopic theory with the experimental observable. Section 5 discusses the standard three-layer model approach, and illustrates the use of the theory in some typical systems. Then, in Section 6 we present a more complete formalism that does not utilize the three-layer approximation. This approach is appropriate for use in the standard supercell/repeated slab representation of the surface, and reduces to that of Ibach and Mills [11] in the limit of a bulklike termination. Local fields are included in a proper fashion, without recourse to effective medium theory corrections.

[1] Among the assumptions of the theory are that the electron cannot penetrate the surface, and that it moves as a classical particle along the specular trajectory.

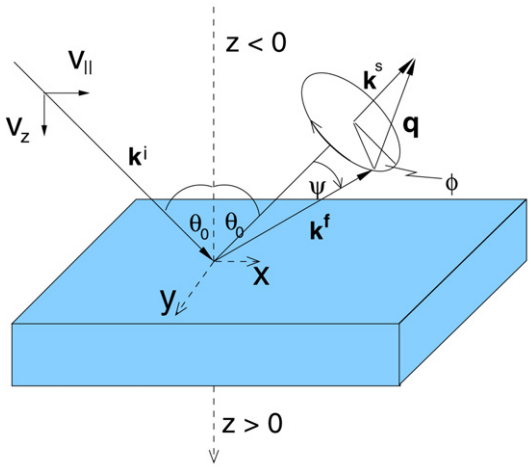

Fig. 1. Geometry of an electron energy loss experiment in the reflection geometry. The incident wavevector $\mathbf{k}^i$ and the specularly reflected wavevector $\mathbf{k}^s$ lie in the x–z plane; θ_0 is the angle of incidence and ψ the deflection angle from $\mathbf{k}^s$.

The local field effect is a *bona fide* many-body interaction, since it originates from the interaction of the scattered electron with the inhomogeneous induced charge density of the other electrons. The influence of other many-body interactions, such as self-energy corrections (which directly influence the electronic bandstructure) and the electron–hole interaction (which may strongly modify the dielectric response function), is considered, in the context of the three-layer model, in Section 5.3.

2. Theory of electron energy loss at surfaces

In a HREELS experiment a low-energy beam of monochromatic electrons (having wavevector $\mathbf{k}^i$ and velocity $\mathbf{v}$) impinges upon a sample, all the while interacting with the atoms on the crystal surface through various elementary excitations. The scattered electrons are collected with a new wavevector $\mathbf{k}^f$, having transferred a momentum $\mathbf{q}$ to the surface. A schematic representation of a typical electron trajectory is shown in Fig. 1. We exploit the semi-infinite geometry and decompose vector quantities $\mathbf{q}$, $\mathbf{r}$ into parallel components $\mathbf{q}_\parallel$, $\mathbf{r}_\parallel$ and normal components q_z, z. The impinging electron acts as an external perturbation, and is represented by a varying charge density,

$$\rho^{\text{ext}}(\mathbf{r},t) = \delta(\mathbf{r}_\parallel - \mathbf{v}_\parallel t)\big[\delta(z - v_z t)\theta(-t) + \delta(z + v_z t)\theta(t)\big] \tag{1}$$

We use $\theta(z)$ to indicate the Heaviside step function, equal to 1 for positive arguments, $1/2$ at the origin and zero elsewhere. The corresponding external potential is given by:

$$\phi^{\text{ext}}(\mathbf{r},t) = \int \mathrm{d}^3\mathbf{r}' \frac{\rho^{\text{ext}}(\mathbf{r}',t)}{|\mathbf{r}-\mathbf{r}'|} \tag{2}$$

After applying two-dimensional Fourier transforms into $(\mathbf{q}_\parallel, \omega)$ space, we arrive, after some algebra, at the following expressions:

$$\rho^{\text{ext}}(\mathbf{q}_\parallel, z, \omega) = \frac{2\theta(-z)}{v_z}\cos(b_\parallel z) \tag{3}$$

$$\phi^{\text{ext}}(\mathbf{q}_\parallel, z, \omega) = \frac{4\pi}{v_z}\frac{1}{b_\parallel^2 + q_\parallel^2}\big\{\theta(-z)\big[2\cos(b_\parallel z) - e^{q_\parallel z}\big] + \theta(z)e^{-q_\parallel z}\big\} \tag{4}$$

where for clarity we have defined

$$b_\parallel = \frac{\omega - \mathbf{q}_\parallel \cdot \mathbf{v}_\parallel}{v_z} \tag{5}$$

According to linear response theory, we can write the scattering cross section in terms of the external potential, given above, and the induced charge density, as:

$$\frac{\mathrm{d}S}{\mathrm{d}(\hbar\omega)\,\mathrm{d}^2\mathbf{q}_\parallel} = \mathrm{Im}\int \mathrm{d}z\,\phi^{\mathrm{ext}}(\mathbf{q}_\parallel, z, \omega)\rho^{\mathrm{ind}}(\mathbf{q}_\parallel, z, \omega) \tag{6}$$

$$= \mathrm{Im}\int \mathrm{d}z\,\rho^{\mathrm{ext}}(\mathbf{q}_\parallel, z, \omega)\big[\phi^{\mathrm{tot}}(\mathbf{q}_\parallel, z, \omega) - \phi^{\mathrm{ext}}(\mathbf{q}_\parallel, z, \omega)\big] \tag{7}$$

Finally, we express this in terms of the inverse dielectric function

$$\frac{\mathrm{d}S}{\mathrm{d}(\hbar\omega)\,\mathrm{d}^2\mathbf{q}_\parallel} = \mathrm{Im}\int \mathrm{d}z\,\rho^{\mathrm{ext}}(\mathbf{q}_\parallel, z, \omega)\int \mathrm{d}z'\big[\varepsilon^{-1}(\mathbf{q}_\parallel, z, z', \omega) - \delta(z - z')\big]\phi^{\mathrm{ext}}(\mathbf{q}_\parallel, z', \omega) \tag{8}$$

If we assume, as done by Ibach and Mills [11], that the electron does not penetrate the solid, we can explicitly write Eq. (8) in the semi-infinite (S.I.) geometry

$$\frac{\mathrm{d}S}{\mathrm{d}(\hbar\omega)\,\mathrm{d}^2\mathbf{q}_\parallel} = \mathrm{Im}\int_{-\infty}^{0} \rho^{\mathrm{ext}}(\mathbf{q}_\parallel, z, \omega)\,\mathrm{d}z\int_{-\infty}^{\infty}\big[\varepsilon^{-1}_{\mathrm{S.I.}}(\mathbf{q}_\parallel, z, z', \omega) - \delta(z - z')\big]\phi^{\mathrm{ext}}(\mathbf{q}_\parallel, z', \omega)\,\mathrm{d}z' \tag{9}$$

Note that experimentally what is measured is the differential scattering cross section, easily obtainable from the following (assuming a small scattering angle [1]):

$$\frac{\mathrm{d}S}{\mathrm{d}(\hbar\omega)\,\mathrm{d}\Omega} = \frac{\mathrm{d}S}{\mathrm{d}(\hbar\omega)\,\mathrm{d}^2\mathbf{q}_\parallel}\frac{\mathrm{d}\mathbf{q}_\parallel}{\mathrm{d}\Omega} = \frac{\mathrm{d}S}{\mathrm{d}(\hbar\omega)\,\mathrm{d}^2\mathbf{q}_\parallel}\frac{m^2 v_z^2}{\hbar^2\cos\theta_0} \tag{10}$$

A first problem is how to calculate $\varepsilon^{-1}_{\mathrm{S.I.}}(\mathbf{q}_\parallel, z, z', \omega)$, the screening appropriate for potentials close to a surface (see below for the various types of screening). A second problem is to adapt Eq. (9) to a repeated slab geometry, which is the standard way for modeling surfaces within a plane-wave framework. Due to the long range Coulomb interaction this is not trivial.

3. The dielectric susceptibility tensor

The response of the system (induced current and charge densities) can be calculated to first order in the external field by means of perturbation theory. In this way we establish a linear relationship between the electric displacement $\mathbf{D}$ and the electric field $\mathbf{E}$:

$$\mathbf{D}(\mathbf{r}, t) = \int \mathrm{d}^3\mathbf{r}'\int_{-\infty}^{t} \mathrm{d}t'\,\overleftrightarrow{\varepsilon}\,(\mathbf{r}, \mathbf{r}', t - t')\cdot\mathbf{E}(\mathbf{r}', t') \tag{11}$$

which defines the dielectric susceptibility tensor $\overleftrightarrow{\varepsilon}\,(\mathbf{r}, \mathbf{r}', t - t')$. Eq. (11) is the most general linear relation which can be written between two vector functions of space and time. The dielectric susceptibility is a property of the unperturbed system and can be calculated, with varying degrees of difficulty, from its wave functions. It depends on $t - t'$ (and not separately on t and t') due to the translational invariance in time of the unperturbed system in the absence of external magnetic fields. Limiting the integration in Eq. (11) to times less than t is imposed by causality, in that the value of $\mathbf{D}$ at time t cannot be affected by the values assumed by $\mathbf{E}$ at later times.

To proceed, we will make use of the fact that Maxwell's equations are greatly simplified in Fourier space. We define the Fourier transform in the following manner:

$$\mathbf{E}(\mathbf{k}, \omega) = \frac{1}{2\pi}\int_{-\infty}^{\infty} \mathrm{d}t\int \mathrm{d}^3\mathbf{r}e^{-i(\mathbf{k}\cdot\mathbf{r} - \omega t)}\mathbf{E}(\mathbf{r}, t) \tag{12}$$

where $\mathbf{k}$ is a generic wavevector. Maxwell's equations in $(\mathbf{k}, \omega)$ space are therefore given by:

$$i\mathbf{k}\cdot\mathbf{D}(\mathbf{k}, \omega) = 4\pi\rho^{\mathrm{ext}}(\mathbf{k}, \omega), \quad \mathbf{k}\cdot\mathbf{B}(\mathbf{k}, \omega) = 0$$
$$\mathbf{k}\times\mathbf{E}(\mathbf{k}, \omega) = \frac{\omega}{c}\mathbf{B}(\mathbf{k}, \omega), \quad i\mathbf{k}\times\mathbf{B}(\mathbf{k}, \omega) = \frac{4\pi}{c}\mathbf{J}^{\mathrm{ext}}(\mathbf{k}, \omega) - \frac{i\omega}{c}\mathbf{D}(\mathbf{k}, \omega) \tag{13}$$

Hence, Eq. (11) becomes

$$\mathbf{D}(\mathbf{k},\omega) = \int \mathrm{d}^3\mathbf{k}' \overleftrightarrow{\varepsilon}(\mathbf{k},\mathbf{k}',\omega)\cdot\mathbf{E}(\mathbf{k}',\omega) \tag{14}$$

with

$$\overleftrightarrow{\varepsilon}(\mathbf{k},\mathbf{k}',\omega) = \int \mathrm{d}^3\mathbf{r}\,\mathrm{d}^3\mathbf{r}' e^{-i(\mathbf{k}\cdot\mathbf{r}-\mathbf{k}'\cdot\mathbf{r}')} \overleftrightarrow{\varepsilon}(\mathbf{r},\mathbf{r}',\omega) \tag{15}$$

Before continuing, we briefly comment on the form of $\overleftrightarrow{\varepsilon}(\mathbf{r},\mathbf{r}',\omega)$. For simplicity, we treat our crystal according to the following approximations: we assume that every electron feels the average field generated by all others; and that the wave functions of the unperturbed system are products of the single particle wave functions. In the presence of a perturbation, every electron feels the external field plus that generated by all the other electrons after perturbation by the same external field (i.e., the induced field). In this way one can arrive at the following form for the components of the dielectric susceptibility tensor [19]:

$$\varepsilon_{\alpha,\beta}(\mathbf{r},\mathbf{r}',\omega) = \delta_{\alpha,\beta}\delta(\mathbf{r}-\mathbf{r}')\left[1-\frac{4\pi e}{m\omega^2}\rho(\mathbf{r})\right] - \frac{4\pi}{\omega^2}\sum_{i,f}\left[\frac{J_\alpha^{if}(\mathbf{r})J_\beta^{fi}(\mathbf{r}')}{\omega+\omega_{if}+i0^+} - \frac{J_\beta^{if}(\mathbf{r}')J_\alpha^{fi}(\mathbf{r})}{\omega-\omega_{if}+i0^+}\right] \tag{16}$$

where i runs over the filled states, f runs over the empty states, and

$$J_\alpha^{if}(\mathbf{r}) = \frac{e\hbar}{2mi}\left[\psi_i^*(\mathbf{r})\frac{\partial}{\partial x_\alpha}\psi_f(\mathbf{r}) - \psi_f(\mathbf{r})\frac{\partial}{\partial x_\alpha}\psi_i^*(\mathbf{r})\right] \tag{17}$$

We have, therefore, an explicit form for the dielectric susceptibility in terms of the single particle wave functions. This approximation, generally called RPA (Random Phase Approximation), completely neglects the effects of exchange and correlation between the electrons, which are important in general. However, we could also start from a more general expression for $\varepsilon_{\alpha,\beta}$, which includes exchange-correlation effects [14,19–22]. Later in this chapter we will demonstrate the importance of such effects by means of an illustrative example.

We now return to the problem of the dielectric response. Let us define the longitudinal component of the electric field (or indeed, of any vector) as

$$\mathbf{E}_L(\mathbf{k},\omega) = \frac{\mathbf{k}}{k}\cdot\mathbf{E}(\mathbf{k},\omega) \tag{18}$$

The first of Maxwell's equations (Eq. (13)) can be written as:

$$ik\mathbf{D}_L(\mathbf{k},\omega) = 4\pi\rho^{\mathrm{ext}}(\mathbf{k},\omega) \tag{19}$$

However, the external field $\mathbf{E}^{\mathrm{ext}}$ also satisfies this equation, and therefore one can identify $\mathbf{D}_L$ with $\mathbf{E}_L^{\mathrm{ext}}$. This obviously does not signify that $\mathbf{D}$ is equal to $\mathbf{E}^{\mathrm{ext}}$, as the transverse components can be different.

Let us now consider the case of an external longitudinal field, which can be described as the gradient of a scalar potential. An example of this type is the field generated by a charge found nearby (or in the static case, anywhere). In this case $\mathbf{E}$ is also longitudinal, insofar as it is the sum of the external longitudinal field and the induced field, which is also longitudinal. Thus,

$$\mathbf{E}(\mathbf{k},\omega) = \frac{\mathbf{k}}{k}\mathbf{E}_L(\mathbf{k},\omega) \tag{20}$$

Substituting this into Eq. (14), and extracting the longitudinal component, we find:

$$\mathbf{D}_L(\mathbf{k},\omega) = \int \mathrm{d}^3\mathbf{k}'\varepsilon_L(\mathbf{k},\mathbf{k}',\omega)\mathbf{E}_L(\mathbf{k},\omega) \tag{21}$$

where the longitudinal dielectric susceptibility,

$$\varepsilon_L(\mathbf{k},\mathbf{k}',\omega) = \frac{\mathbf{k}}{k}\cdot\overleftrightarrow{\varepsilon}(\mathbf{k},\mathbf{k}',\omega)\cdot\frac{\mathbf{k}'}{k'} \tag{22}$$

describes the longitudinal response ($\mathbf{D}_L$) to a longitudinal field. Remembering that

$$\mathbf{D}_L(\mathbf{k},\omega) = \mathbf{E}_L^{\mathrm{ext}}(\mathbf{k},\omega) = -ik\phi^{\mathrm{ext}}(\mathbf{k},\omega) \tag{23}$$

and that $\mathbf{E}_L(\mathbf{k},\omega) = -ik\phi(\mathbf{k},\omega)$, we obtain the relation between the external potential and the total one:

$$\phi^{\text{ext}}(\mathbf{k},\omega) = \int \mathrm{d}^3\mathbf{k}'\varepsilon_P(\mathbf{k},\mathbf{k}',\omega)\phi(\mathbf{k}',\omega) \tag{24}$$

with

$$\varepsilon_P(\mathbf{k},\mathbf{k}',\omega) = \frac{k'}{k}\varepsilon_L(\mathbf{k},\mathbf{k}',\omega) \tag{25}$$

The susceptibility $\varepsilon_P(\mathbf{k},\mathbf{k}',\omega)$ describes the response to a potential and is related to $\overleftrightarrow{\varepsilon}$ by means of Eq. (22). Once the inverse of ε_P is known, it is then possible to describe how the external potential is screened. In fact, solving Eq. (24) with respect to ϕ one finds:

$$\phi(\mathbf{k},\omega) = \int \mathrm{d}^3\mathbf{k}'\varepsilon_P^{-1}(\mathbf{k},\mathbf{k}',\omega)\phi^{\text{ext}}(\mathbf{k}',\omega) \tag{26}$$

where ε_P^{-1} is defined from the following equation:

$$\int \mathrm{d}^3\mathbf{k}''\varepsilon_P(\mathbf{k},\mathbf{k}'',\omega)\varepsilon_P^{-1}(\mathbf{k}'',\mathbf{k}',\omega) = \delta(\mathbf{k}-\mathbf{k}') \tag{27}$$

Given the external potential $\phi^{\text{ext}}(\mathbf{k},\omega)$, one can use Eq. (24) to calculate the total potential ϕ for any system. This is greatly simplified in the case of an infinite crystal with a weakly inhomogeneous charge density, where local-field effects can be neglected. In this case the kernel ε_P becomes diagonal, and Eq. (24) reduces to a multiplicative expression.

In the previous discussion of linear response theory, we instead could have calculated (for the case of an external longitudinal field) the *induced* charge, and from this, the induced potential. In this manner we directly calculate ε_P, rather than the tensor $\varepsilon_{\alpha,\beta}$. In the RPA, ε_P is given by [23]:

$$\varepsilon_P(\mathbf{k},\mathbf{k}',\omega) = \delta(\mathbf{k}-\mathbf{k}') + \frac{4\pi e^2}{k^2}\sum_{i,f}\left[\frac{\langle i|e^{-i\mathbf{k}\cdot\mathbf{r}}|f\rangle\langle f|e^{i\mathbf{k}'\cdot\mathbf{r}}|i\rangle}{\omega_{fi}-\omega-i0^+} + \frac{\langle i|e^{i\mathbf{k}'\cdot\mathbf{r}}|f\rangle\langle f|e^{-i\mathbf{k}\cdot\mathbf{r}}|i\rangle}{\omega_{fi}+\omega+i0^+}\right] \tag{28}$$

One can show using gauge invariance and charge conservation that Eqs. (22) and (25) are equivalent to Eq. (28).

In infinite crystals it is often preferable to calculate ε_P rather than the tensor $\overleftrightarrow{\varepsilon}$. This is because ε_P is more simple to calculate (see Eq. (28)), and yet describes all the dielectric properties of an infinite cubic crystal. In fact, it clearly describes the dielectric screening, whereas the optical properties are described by the transverse dielectric susceptibility. One can demonstrate, however, in the limit of long wavelength, that the transverse susceptibility is equal to the longitudinal one, so that the latter can actually be calculated from ε_P.

The situation is different in a finite crystal. The presence of a surface breaks the isotropy of the system, and the transverse susceptibility is in general different from the longitudinal one. The scalars ε_P and ε_L, and the components of $\overleftrightarrow{\varepsilon}$, are all different from one another. Macroscopic local field effects arise from the different susceptibilities of vacuum and crystal. In the case of the optical properties, it is necessary to use the tensor $\overleftrightarrow{\varepsilon}$, and not just ε_P or ε_L. Moreover, we will see in the next section that the Cartesian components of $\overleftrightarrow{\varepsilon}$ (i.e., $\varepsilon_{\alpha,\beta}$) behave differently from ε_L inside the crystal, in that they reach their "bulk" value after only a few atomic layers below the surface: this does not happen for ε_L or ε_P.

4. Dielectric response in semi-infinite systems

4.1. Screening of an external potential

Screening of the potential generated by a charge situated close to the surface of a crystal is described by Eq. (28). Calculation of the effective potential ϕ is complicated, however, because of the difficulty involved in calculating ε_P^{-1}. Much work has been carried out for the extremely idealized case of jellium, but little in more realistic cases [12,24]. An alternative strategy is to construct a simple model of the dielectric tensor, and from this calculate the screening.

In order to investigate the different behavior of ε_P and $\overleftrightarrow{\varepsilon}$ as a function of the distance from the surface, we will consider the following very simple model of $\overleftrightarrow{\varepsilon}$, corresponding to a sharp termination of a classical dielectric:

$$\varepsilon_{\alpha,\beta}(\mathbf{r},\mathbf{r}') = \delta_{\alpha,\beta}\delta(\mathbf{r}-\mathbf{r}')\big[1+(\varepsilon_b-1)\theta(z)\big] \tag{29}$$

By combining Eqs. (22) and (25) with the Fourier transform of Eq. (29) we can obtain ε_P. The result is:

$$\varepsilon_P(\mathbf{k},\mathbf{k}') = \delta(\mathbf{k}-\mathbf{k}') + \frac{2i(\varepsilon_b-1)}{4\pi}\frac{\mathbf{k}\cdot\mathbf{k}'}{k^2}\delta(\mathbf{k}_\parallel-\mathbf{k}'_\parallel)\frac{1}{k'_z-k_z+i\eta} \tag{30}$$

with $\eta\to 0^+$ (the fraction is the Fourier transform of the step function). Taking the inverse Fourier transform, and integrating in the complex plane, we obtain:

$$\varepsilon_P(\mathbf{r},\mathbf{r}') = \delta(\mathbf{r}-\mathbf{r}')\big[1+(\varepsilon_b-1)\theta(z)\big] - \frac{\varepsilon_b-1}{4\pi}\frac{z\delta(z')}{(|\mathbf{r}_\parallel-\mathbf{r}'_\parallel|^2+z^2)^{\frac{3}{2}}} \tag{31}$$

This expression is composed of a long range term (the second term) that modifies the screening properties, with respect to those of an infinite crystal (the first term), even at fairly large distances from the surface. We will see that this term is connected with the image potential of classical electrostatics.

To describe the screening of an external potential, we need to invert Eq. (31). This can most easily be done by keeping the coordinates parallel to the surface in $\mathbf{k}$ space:

$$\varepsilon_P(\mathbf{k}_\parallel,\mathbf{k}'_\parallel,z,z') = \delta(\mathbf{k}_\parallel-\mathbf{k}'_\parallel)\left[\delta(z-z')\big[1+(\varepsilon_b-1)\theta(z)\big] - \frac{\varepsilon_b-1}{2}\operatorname{sgn}(z)\delta(z')e^{-k_\parallel|z|}\right] \tag{32}$$

The inverse of ε_P is easily found in this representation:

$$\varepsilon_P^{-1}(\mathbf{k}_\parallel,\mathbf{k}'_\parallel,z,z') = \frac{\delta(\mathbf{k}_\parallel-\mathbf{k}'_\parallel)}{[1+(\varepsilon_b-1)\theta(z)]}\left[\delta(z-z') + \frac{\varepsilon_b-1}{\varepsilon_b+1}\operatorname{sgn}(z)\delta(z')e^{-k_\parallel|z|}\right]. \tag{33}$$

Again, we see that there is a long range contribution, given by the last term.

4.2. Charge inside a crystal

We can also consider a charge placed inside a crystal, at $\mathbf{r}_\parallel=0$, $z=z_0>0$. The Coulomb potential generated by this charge, as a function of $\mathbf{k}_\parallel$ and z, is given by:

$$\phi^{\text{ext}}(\mathbf{k}_\parallel,z) = \frac{2\pi e}{k_\parallel}e^{-k_\parallel|z-z_0|} \tag{34}$$

From the expressions presented previously, it is straightforward to obtain the total potential:

$$\phi(\mathbf{k}_\parallel,z) = \int_{-\infty}^{\infty}\mathrm{d}z'\int \mathrm{d}^2\mathbf{k}'_\parallel\,\varepsilon_P^{-1}(\mathbf{k}_\parallel,\mathbf{k}'_\parallel,z,z')\phi^{\text{ext}}(\mathbf{k}'_\parallel,z') \tag{35}$$

$$= \frac{2\pi e}{k_\parallel[1+(\varepsilon_b-1)\theta(z)]}\left[e^{-k_\parallel|z-z_0|} + \frac{\varepsilon_b-1}{\varepsilon_b+1}\operatorname{sgn}(z)\delta(z')e^{-k_\parallel(|z|+z_0)}\right] \tag{36}$$

The potential in real space can be obtained by performing the inverse Fourier transform of this equation. After extending the integral into the complex plane, we find the following:

$$z>0,\quad \phi(\mathbf{r}) = \frac{e}{\varepsilon_b|\mathbf{r}-\mathbf{r}_0|} + \frac{1}{\varepsilon_b}\frac{\varepsilon_b-1}{\varepsilon_b+1}\frac{e}{[r_\parallel^2+(z+z_0)^2]^{\frac{1}{2}}} \tag{37}$$

$$z<0,\quad \phi(\mathbf{r}) = \frac{2e}{\varepsilon_b+1}\frac{1}{|\mathbf{r}-\mathbf{r}_0|} \tag{38}$$

This result coincides with that obtained in classical electrostatics using the method of image charges. The corresponding formulae for a charge outside the crystal can be obtained in a similar manner:

$$z > 0, \quad \phi(\mathbf{r}) = \frac{2e}{\varepsilon_b + 1} \frac{1}{|\mathbf{r} - \mathbf{r}_0|} \tag{39}$$

$$z < 0, \quad \phi(\mathbf{r}) = \frac{e}{|\mathbf{r} - \mathbf{r}_0|} - \frac{\varepsilon_b - 1}{\varepsilon_b + 1} \frac{e}{[r_\parallel^2 + (z + z_0)^2]^{\frac{1}{2}}} \tag{40}$$

It is now clear why $\varepsilon_P(\mathbf{r}, \mathbf{r}')$ contains a long range term: it derives from the charge induced at the surface that generates a Coulomb potential at long range. It also appears appropriate that the Cartesian components of $\overleftrightarrow{\varepsilon}$ do not have a similar term in this case. Indeed, it is likely that the relationship between **P** and **E** (and therefore between **D** and **E**) is quasi-local, from the fact that the atoms polarize in response to the nearby (local) electric field. This is obvious within a model of independent atoms, but it can be demonstrated for the more general case if the wave functions in Eq. (28) are expanded in terms of Wannier functions [23,21]: after some atomic layers below the surface, the dielectric susceptibility of an infinite crystal is recovered.

One can understand the different behavior of ε_P and $\overleftrightarrow{\varepsilon}$ by observing that the latter expresses the relation between **P** and **E** (which is quasi local), while the former expresses the relationship between the external potential and the induced one, with important effects due to charges induced at the surface. It is not surprising that this second relation is much less local than the first.

5. Model calculations of electron energy loss

5.1. Bulklike-terminated surface

Having derived an expression for the dielectric susceptibility appropriate for screening potentials in the simple model system described by Eq. (29), it is now quite straightforward to obtain an expression for the electron energy loss function. We substitute $\varepsilon_{\mathrm{P}}^{-1}(\mathbf{q}_\parallel, z, z', \omega)$ for the dielectric susceptibility of the semi-infinite crystal $\varepsilon_{\mathrm{S.I.}}^{-1}(\mathbf{q}_\parallel, z, z', \omega)$ appearing in Eq. (9), along with the Fourier transformed expressions for the external charge (Eq. (1)) and potential (Eq. (2)) that determine the experimental kinematic setup. The differential scattering cross section reduces to the familiar expression found in the literature (see [11] and references therein):

$$\frac{\mathrm{d}S}{\mathrm{d}(\hbar\omega)\,\mathrm{d}\Omega} = \frac{2}{\pi^2} \frac{1}{\cos\theta_0} \frac{|\mathbf{k}^f|}{|\mathbf{k}^i|} \frac{|\mathbf{q}_\parallel|}{|\mathbf{q}_\parallel^2 + q_z^2|^2} \operatorname{Im}\left\{ \frac{-2}{1 + \varepsilon_b} \right\} \equiv A\left(\mathbf{k}^i, \mathbf{k}^f\right) \operatorname{Im} g(\mathbf{q}_\parallel, \omega) \tag{41}$$

which is often expressed as the product of two terms, as shown ($\mathbf{q}_\parallel = \mathbf{k}_\parallel^i - \mathbf{k}_\parallel^f$). The first of these, the kinematic prefactor $A(\mathbf{k}^i, \mathbf{k}^f)$, depends on the trajectory of the incident electron. The second term is the so-called loss function $\operatorname{Im} g(\mathbf{q}_\parallel, \omega)$ that contains all the information concerning the interaction between the external charge and the crystal. For the present simple model of the semi-infinite crystal, the loss function is simply given by the (inverse) average of the dielectric functions of vacuum (1) and bulk (ε_b).

In Fig. 2 we compare some experimental EELS data measured on the Si(100)–(2 × 1) surface with the results of a calculation using Eq. (41). For ε_b we use a bulk Si spectrum computed *ab initio* within DFT-LDA at the RPA level; calculations were performed at a 15 Ry kinetic energy cutoff and sampled 50 000 random **k**-points in the first Brillouin zone. From the figure we see that Eq. (41) does in fact succeed in reproducing some of the peaks observed in the experimental spectra, such as the interband scattering peaks near the E_1 (∼3.4 eV) and E_2 (∼5.0 eV) critical point energies. However, the low energy structures ($\hbar\omega < 2.0$ eV) are missing due to the neglect of the true surface geometry and associated electronic states. Furthermore, the surface plasmon peak position [occurring where $\varepsilon_b = -1$ (∼11.2 eV)] is not accurately described within RPA: quantitative prediction of the latter requires an improved treatment of many-body effects as shown by Olevano and Reining [25] and Silkin et al. [24].

5.2. Anisotropic three-layer model

The natural extension of the previous treatment is to consider a three-layer system, such that the surface region is more accurately described by its own dielectric tensor ε_s. This was first carried out by Ibach and colleagues [11,10] assuming an isotropic surface layer. A more precise treatment was offered by Selloni and Del Sole [12] who solved

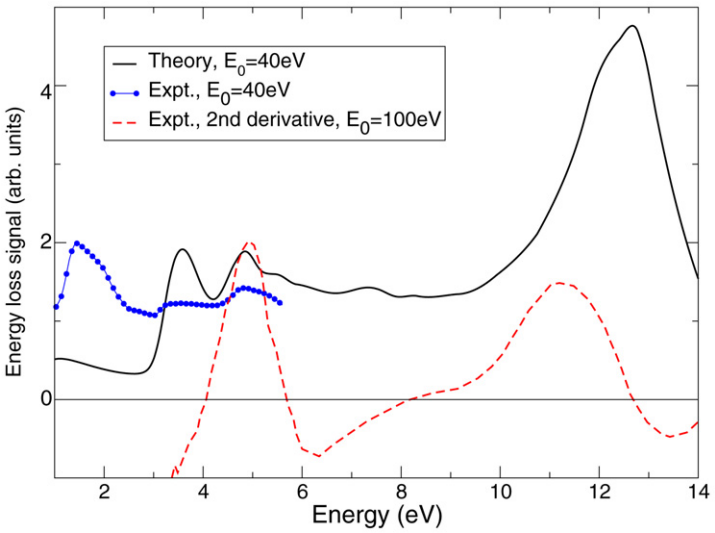

Fig. 2. Electron energy loss spectrum of Si(100)–$p(2 \times 1)$, computed using the model loss function of Eq. (41), compared with the experimental data of Farrell et al. [26] ($E_0 = 40$ eV; $\theta_0 = 60°$; $\psi = 0°$) and the second derivative data of Ibach and Rowe [27] ($E_0 = 100$ eV; $\theta_0 = 0°$; $\psi = 42°$).

Poisson's equation for the total field within an anisotropic, yet local, three-layer model. They obtained the following expression for the loss function as a function of the transferred momentum and energy:

$$\operatorname{Im} g(\mathbf{q}_\parallel, \omega) = \operatorname{Im}\left\{\frac{-2}{1 + \varepsilon_{\text{eff}}(\mathbf{q}_\parallel, \omega)}\right\} \tag{42}$$

Hence the bulk dielectric function appearing in Eq. (41) is substituted by an effective dielectric function $\varepsilon_{\text{eff}}(\mathbf{q}_\parallel, \omega)$ which describes the dielectric properties of the surface and underlying bulk layers.

Assuming that scattering occurs in the x–z plane (see Fig. 1), the effective dielectric function is found to be [12]:

$$\varepsilon_{\text{eff}}(\mathbf{q}_\parallel, \omega) = \varepsilon_s \frac{\varepsilon_s + \varepsilon_b + (\varepsilon_b - \varepsilon_s)e^{-2q_\parallel d_s \sqrt{\varepsilon_{sx}/\varepsilon_{sz}}}}{\varepsilon_s + \varepsilon_b - (\varepsilon_b - \varepsilon_s)e^{-2q_\parallel d_s \sqrt{\varepsilon_{sx}/\varepsilon_{sz}}}} \tag{43}$$

where $\varepsilon_s = \sqrt{\varepsilon_{sx}\varepsilon_{sz}}$, d_s is the surface layer thickness, and ε_{sx} and ε_{sz} are the components of the surface dielectric tensor parallel to the x direction, which lies in the surface plane, and to the z direction, perpendicular to the surface, respectively.

The effective dielectric function $\varepsilon_{\text{eff}}(\mathbf{q}_\parallel, \omega)$ is a combination of the surface (ε_{sx}, ε_{sz}) and bulk dielectric functions (ε_b). Here we present a more transparent, although equivalent, formula than in [12]. Eq. (43) recovers two well known limits: for $\mathbf{q}_\parallel \to 0$, $\varepsilon_{\text{eff}}(\mathbf{q}_\parallel, \omega)$ tends to ε_b. This because the field of the incident electron, decaying as $\exp(-q_\parallel z)$, penetrates deeply into the bulk, so that the surface layer has only a small effect on the loss function. Taking into account first order terms in $q_\parallel d_s$, we get the first order expansion $\varepsilon_{\text{eff}}(\mathbf{q}_\parallel, \omega) \simeq \varepsilon_b + q_\parallel d_s(\varepsilon_{sx} - \varepsilon_b^2/\varepsilon_{sz})$, as in [12]. On the contrary, for very large $\mathbf{q}_\parallel$, $\varepsilon_{\text{eff}}(\mathbf{q}_\parallel, \omega)$ tends to ε_s: EELS, in this case is a true probe of the surface layers. The main structure in Eq. (42), the surface plasmon, occurs when the denominator vanishes (no bulk plasmon is derived within this theory, because of the assumption that electrons do not penetrate the sample). In the case of a perfect bulk termination, $\varepsilon_{\text{eff}} \equiv \varepsilon_b$, and the usual surface plasmon dispersion is recovered: $\varepsilon_b(\omega) = -1$ [11]. The presence of the surface layer affects this dispersion, which becomes $\varepsilon_{\text{eff}}(\mathbf{q}_\parallel, \omega) = -1$. In the final section of this chapter we will show an example of the success of this formalism within the RPA. First, however, we discuss briefly the effect of going beyond the RPA when computing EELS.

5.3. Self-energy and excitonic effects

We have seen how the HREELS signal contains structures deriving from peaks in the imaginary part of $\varepsilon_{\text{eff}}(\mathbf{q}_\parallel, \omega)$, i.e., related to interband transitions, in addition to the surface plasmon peak. At these energies, other many-body effects

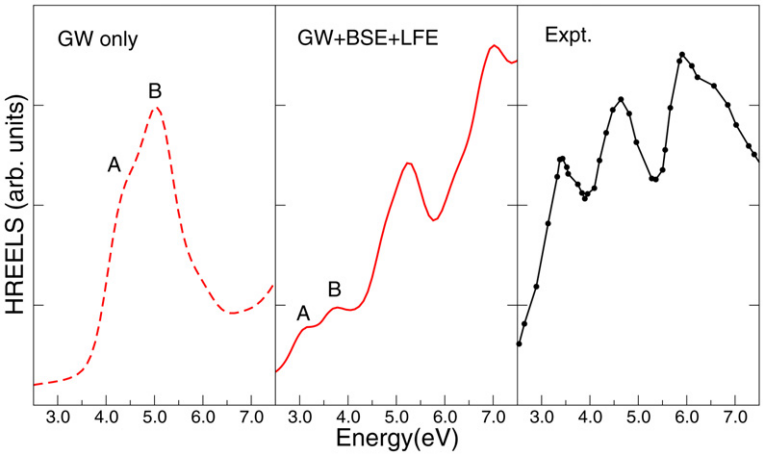

Fig. 3. Electron energy loss spectra of the C(100)–(2 × 1) surface. Left: theoretical spectrum calculated including self-energy effects (GW) only. Middle: spectrum calculated with self-energy, local field and excitonic effects included (GW+LFE+EXC). Right: experimental spectrum from [30]. The peaks A and B correspond to the two lower energy peaks in the experiment. Theoretical spectra are from [14].

(in particular, self-energy corrections and the electron–hole interaction), can play an important role. As mentioned earlier, our treatment of HREELS can incorporate such effects by considering a more advanced expression for $\varepsilon_{\alpha,\beta}$ than the RPA one (Eq. (16)), or, in the context of the three-layer model, a more precise treatment of ε_s and ε_b. Self energy and excitonic effects can be included using the Green's function formalism by applying the so-called GW method for calculating the quasi-particle band structures, and by solving the Bethe–Salpeter equation to account for the creation of electron–hole excitations. A detailed description of the method can be found, e.g., in [29], as well as in other chapters of this volume. For completeness, we briefly mention the main equations used to calculate the quasi-particle energies and the dielectric response beyond the independent-particle approximation.

Starting from eigenvalues and eigenfunctions obtained within a DFT calculation in a Kohn–Sham (KS) formulation, the real quasi-particle energies can be calculated in a first-order perturbative approach (the GW method), as:

$$\epsilon_i^{QP} = \epsilon_i^{KS} + \frac{1}{1+\beta_i}\langle\varphi_i^{KS}|\,\Sigma\big(\epsilon_i^{KS}\big) - V_{xc}\,|\varphi_i^{KS}\rangle \tag{44}$$

Here V_{xc} is the exchange-correlation potential of the DFT-KS self-consistent equations, $\Sigma = iGW$ is the non-Hermitian, non-local, energy dependent self-energy operator, and β_i is the linear coefficient in the energy expansion of Σ around the KS energies.

Once the quasi-particle states are obtained, the dielectric response including electron–hole excitations can be calculated by solving the Bethe–Salpeter equation. In the usual formulation, this reduces to solving an eigenvalue problem for an excitonic Hamiltonian:

$$\begin{aligned} H_{exc}^{(n_1,n_2),(n_3,n_4)} &= \big(\epsilon_{n_2}^{QP} - \epsilon_{n_1}^{QP}\big)\delta_{n_1,n_3}\delta_{n_2,n_4} \\ &\quad - (f_{n_2} - f_{n_1}) \int \mathrm{d}\mathbf{r}_1\,\mathrm{d}\mathbf{r}_1'\,\mathrm{d}\mathbf{r}_2\,\mathrm{d}\mathbf{r}_2'\phi_{n_1}(\mathbf{r}_1)\phi_{n_2}^*(\mathbf{r}_1')\Xi(\mathbf{r}_1,\mathbf{r}_1',\mathbf{r}_2,\mathbf{r}_2')\phi_{n_3}^*(\mathbf{r}_2)\phi_{n_4}(\mathbf{r}_2') \end{aligned} \tag{45}$$

where n_i are energy and momentum indices for the Kohn–Sham states. The kernel Ξ contains two contributions: $\bar{v}$, which is the bare Coulomb interaction with the long-range part ($\mathbf{q} \to 0$) removed ($\bar{v}$ describes local-field effects); and W, the attractive screened Coulomb electron–hole interaction.

In order to illustrate the importance of many-body effects in HREELS spectra, we report here our results obtained for the C(100) surface within the three-layer scheme. Note that, in practical calculations, it is usually desirable to replace the $\mathbf{q}_\parallel$-dependent surface dielectric functions appearing in Eq. (43) with the *optical* ones, i.e., in the limit of small $\mathbf{q}$, which are more easily calculated. Within this approximation the $\mathbf{q}_\parallel$-dependence of $\varepsilon_{\mathrm{eff}}(\mathbf{q}_\parallel,\omega)$ originates only from the averaging procedure over surface and bulk regions. We also mention here a practical issue that arises when including local field effects through Eq. (45) within a repeated slab (supercell) framework, which is the standard way to treat surfaces in practical *ab initio* calculations. The direct output of such calculations is the repeated slab (RS)

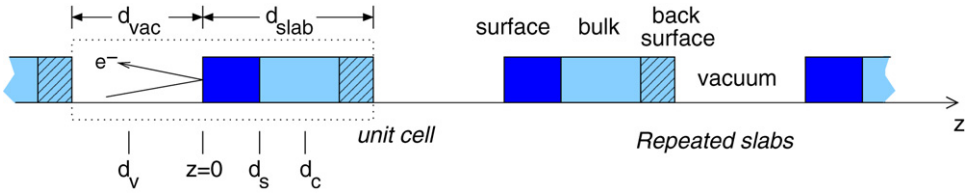

Fig. 4. HREELS in a repeated slab geometry. In a three-layer approach, the surface is modeled using an effective dielectric function ε_s corresponding to the region $0 < z < d_s$. In the extended model, d_s is not used, but rather a cut-off parameter d_c whose value is simply limited by the slab thickness.

dielectric response; what is required to model the surface, however, is the response of a single slab (SS). This can be extracted from the RS data using the following expressions derived within effective medium theory [31]:

$$\varepsilon_{\parallel}^{SS}(\omega) = \varepsilon_{\parallel}^{RS}\frac{(d_{\text{vac}} + d_{\text{slab}})}{d_{\text{slab}}} - \frac{d_{\text{vac}}}{d_{\text{slab}}} \quad \text{and} \quad \frac{1}{\varepsilon_{\perp}^{SS}(\omega)} = \frac{1}{\varepsilon_{\perp}^{RS}}\frac{(d_{\text{vac}} + d_{\text{slab}})}{d_{\text{slab}}} - \frac{d_{\text{vac}}}{d_{\text{slab}}} \tag{46}$$

See Fig. 4 for an explanation of the various parameters occurring in a repeated slab geometry. In the C(100) calculation, slabs of thickness $d_{\text{slab}} = 16.2$ Å, separated by a fairly thick vacuum region ($d_{\text{vac}} = 10.8$ Å), were considered [14]. The surface dielectric functions are thus obtained by subtracting the bulk contribution from the single-slab dielectric functions, having assumed a surface layer thickness of about $d_s = 3.5$ Å.

In Fig. 3 the experimental HREELS spectrum of the C(100) surface [30] is compared with theoretical spectra obtained at different levels of approximation [14]. It is clear from the figure that a good agreement with theory (in particular, reproducing the three peaks in the experimental spectrum) can only be obtained if a comprehensive treatment of self-energy, excitonic and local field effects is considered. Nevertheless, having to combine an *ab initio* formulation with a classical approach (Eqs. (46)) is not very satisfactory. Furthermore, only symmetric slabs having two equivalent surfaces can be treated in this manner. In the following section, we will consider an alternative scheme that avoids these issues.

6. Extended model of HREELS

6.1. Repeated slab geometry

The anisotropic three-layer model as presented up to now is quite an effective approach for modeling electron energy loss spectroscopy at surfaces. However, as mentioned above, there are a number of drawbacks associated with the scheme. One critical drawback is that an assumption needs to be made regarding the thickness d_s of the surface layer. Of course, it is already an approximation to sharply partition the dielectric response of a slab into a surface and bulk part, since for large $\mathbf{q}_{\parallel}$ the response may vary greatly with the z coordinate. In addition, ε_s is assumed to be local, when in fact it is a function of z and z'.

In this section, therefore, we present a framework for embedding the dielectric response of a repeated slab directly into the general equation describing HREELS in the dipole approximation (Eq. (9)). No assumptions need to be made about the surface layer thickness, so long as a sufficiently thick slab is used in practical calculations. Furthermore, the non-locality of $\varepsilon_P^{-1}(\mathbf{q}_{\parallel}, z, z', \omega)$ is maintained in the formula, and local field effects perpendicular to the surface are naturally included.

We tackle Eq. (9) by making some observations about the real-space behavior of $\varepsilon^{-1}(\mathbf{q}_{\parallel}, z, z', \omega)$. We split the response into two regimes, depending on whether the impinging electron is far from the surface ($z < d_v$), or is close to the surface ($d_v < z < 0$) (see Fig. 4):

$$\frac{\mathrm{d}S}{\mathrm{d}(\hbar\omega)\,\mathrm{d}^2\mathbf{q}_{\parallel}} = \frac{\mathrm{d}S^{\text{FAR}}}{\mathrm{d}(\hbar\omega)\,\mathrm{d}^2\mathbf{q}_{\parallel}} + \frac{\mathrm{d}S^{\text{NEAR}}}{\mathrm{d}(\hbar\omega)\,\mathrm{d}^2\mathbf{q}_{\parallel}} \tag{47}$$

Far from the surface, we make the assumption that the perturbing electron does not see the local atomic structure and fluctuations on the atomic scale. Hence, the dielectric function of the system beyond this point is approximated by the classical truncated *bulk* dielectric function ε_0 (in the following we remove the frequency dependence for clarity):

$$\frac{\mathrm{d}S^{\mathrm{FAR}}}{\mathrm{d}(\hbar\omega)\,\mathrm{d}^2\mathbf{q}_\parallel} = \mathrm{Im}\int_{-\infty}^{d_v} \rho^{\mathrm{ext}}(\mathbf{q}_\parallel, z)\,\mathrm{d}z \int_{-\infty}^{\infty} \big[\varepsilon_0^{-1}(\mathbf{q}_\parallel, z, z') - \delta(z-z')\big]\phi^{\mathrm{ext}}(\mathbf{q}_\parallel, z')\,\mathrm{d}z' \tag{48}$$

which reduces to (substituting for ρ^{ext} and ϕ^{ext} as before),

$$\frac{\mathrm{d}S^{\mathrm{FAR}}}{\mathrm{d}(\hbar\omega)\,\mathrm{d}^2\mathbf{q}_\parallel} = \mathrm{Im}\left\{-\frac{8\pi}{v_z^2}\frac{1}{[b_\parallel^2+q_\parallel^2]^2}\frac{\varepsilon_b-1}{\varepsilon_b+1}e^{-q_\parallel d_v}\big[q_\parallel\cos(b_\parallel d_v) - b_\parallel\sin(b_\parallel d_v)\big]\right\} \tag{49}$$

This term reduces to the familiar expression of Mills in the limit $d_v \to 0$.

Near to the surface, we make use of the observation that $\varepsilon_{\mathrm{S.I.}}^{-1}(\mathbf{q}_\parallel, z, z')$ is short ranged in z and z'. Hence, for $d_v < z < 0$ the integral of z' over all space can be reduced to an integral from d_v to some distance d_c, beyond which $\varepsilon_{\mathrm{S.I.}}^{-1}(\mathbf{q}_\parallel, z, z')$ reduces to the bulk value ε_b. At this point we can therefore replace $\varepsilon_{\mathrm{S.I.}}^{-1}(\mathbf{q}_\parallel, z, z')$ by $\varepsilon_{\mathrm{slab}}^{-1}(\mathbf{q}_\parallel, z, z')$, making sure to chose d_c to be at least half the slab thickness.

$$\frac{\mathrm{d}S^{\mathrm{NEAR}}}{\mathrm{d}(\hbar\omega)\,\mathrm{d}^2\mathbf{q}_\parallel} = \mathrm{Im}\int_{d_v}^{0} \rho^{\mathrm{ext}}(\mathbf{q}_\parallel, z)\,\mathrm{d}z \int_{d_v}^{d_c} \big[\varepsilon_{\mathrm{slab}}^{-1}(\mathbf{q}_\parallel, z, z') - \delta(z-z')\big]\phi^{\mathrm{ext}}(\mathbf{q}_\parallel, z')\,\mathrm{d}z' \tag{50}$$

Once again, making use of Eqs. (1) and (2), we arrive, after some algebra, at the following:

$$\begin{aligned}\frac{\mathrm{d}S^{\mathrm{NEAR}}}{\mathrm{d}(\hbar\omega)\,\mathrm{d}^2\mathbf{q}_\parallel} = \mathrm{Im}\,&\frac{-8\pi}{v_z^2}\frac{1}{b_\parallel^2+q_\parallel^2}\int_{d_v}^{0}\cos(b_\parallel z)\,\mathrm{d}z \\ &\times\left[\int_{d_v}^{0}\varepsilon_{\mathrm{slab}}^{-1}(\mathbf{q}_\parallel, z, z')\big[2\cos(b_\parallel z') - e^{q_\parallel z'}\big]\,\mathrm{d}z' + \int_{0}^{d_c}\varepsilon_{\mathrm{slab}}^{-1}(\mathbf{q}_\parallel, z, z')e^{-q_\parallel z'}\,\mathrm{d}z'\right]\end{aligned} \tag{51}$$

In summary, we transform the back part of the slab into a semi-infinite perfect crystal, avoiding all problems related to the back surface and replicas of repeated slabs.

6.2. Numerical implementation

The remaining practical difficulty in evaluating Eq. (51) lies in the double integrals of $\varepsilon_{\mathrm{slab}}^{-1}(\mathbf{q}_\parallel, z, z')$ over z and z'. In a plane-wave basis set, we can address this by rewriting $\varepsilon_{\mathrm{slab}}^{-1}(\mathbf{q}_\parallel, z, z')$ in terms of the dielectric matrix $\varepsilon_{\mathbf{G},\mathbf{G}'}^{-1}(\mathbf{q})$, which is a quantity easily accessible from excited state codes that use a plane-wave basis (e.g. Yambo [32] or EXC [33]). Furthermore we make the approximation that local fields parallel to the surface are negligible, i.e., $\mathbf{G}_\parallel = \mathbf{G}'_\parallel$ [24]. The 1-D Fourier transform of $\varepsilon_{\mathrm{slab}}^{-1}(\mathbf{q}_\parallel, z, z')$ along z and z' is:

$$\varepsilon_{\mathrm{slab}}^{-1}(\mathbf{q}_\parallel, z, z') = \int_{\mathrm{BZ}}\frac{\mathrm{d}q_z}{2\pi}\sum_{G_z G'_z} e^{i(q_z+G_z)z}\varepsilon_{\mathrm{slab}}^{-1}(\mathbf{q}, G_z, G'_z, \omega)e^{-i(q_z+G'_z)z'} \tag{52}$$

For a sufficiently thick supercell, the replacement

$$\int_{\mathrm{BZ}}\mathrm{d}q_z\, f(q_z) \to \sum_i f\big(q_z^i\big)w\big(q_z^i\big) \approx f\big(q_z^0\big)/d_{\mathrm{cell}} \tag{53}$$

is a reasonable approximation (d_{cell} is the supercell height). Hence,

$$\varepsilon_{\mathrm{slab}}^{-1}(\mathbf{q}_\parallel, z, z') = \frac{1}{2\pi\, d_{\mathrm{cell}}}\sum_{G_z G'_z} e^{i(q_z^0+G_z)z}\varepsilon_{\mathrm{slab}}^{-1}(\mathbf{q}, G_z, G'_z, \omega)e^{-i(q_z^0+G'_z)z'} \tag{54}$$

On performing the Fourier transform, $\varepsilon^{-1}_{\text{slab}}(\mathbf{q}_\parallel, z, z', \omega)$ can be moved outside the integrals over z and z' in Eq. (51), allowing the expression to be evaluated analytically. Following some more tedious but simple algebra, we arrive at the final expression for the scattering cross section:

$$\begin{aligned}\frac{\mathrm{d}S}{\mathrm{d}(\hbar\omega)\,\mathrm{d}^2\mathbf{q}_\parallel} &= \operatorname{Im}\frac{-8\pi}{v_z^2}\frac{1}{[b_\parallel^2+q_\parallel^2]^2}\frac{\varepsilon_b-1}{\varepsilon_b+1}e^{-q_\parallel d_v}\big[q_\parallel\cos(b_\parallel d_v)-b_\parallel\sin(b_\parallel d_v)\big]\\ &\quad+\operatorname{Im}\frac{-8\pi}{v_z^2}\frac{1}{b_\parallel^2+q_\parallel^2}\frac{1}{d_{\text{cell}}}\sum_{G_z}\left|\frac{e^{[i(q_z^0+G_z)]z}}{b_\parallel^2+[i(q_z^0+G_z)]^2}\left\{\big[i\big(q_z^0+G_z\big)\big]\cos(b_\parallel z)+b_\parallel\sin(b_\parallel z)\right\}\right|_{d_v}^{0}\\ &\quad\times\sum_{G'_z}\varepsilon^{-1}_{\text{slab}}\big(\mathbf{q}_\parallel+\mathbf{G}_\parallel,q_z^0+G_z,q_z^0+G'_z,\omega\big)\left\{\left|\frac{e^{[-q_\parallel-i(q_z^0+G'_z)]z}}{-q_\parallel-i(q_z^0+G_z)]}\right|_0^{d_c}-\left|\frac{e^{[+q_\parallel-i(q_z^0+G'_z)]z}}{+q_\parallel-i(q_z^0+G_z)]}\right|_{d_v}^{0}\right.\\ &\quad\left.+2\left|\frac{e^{[-i(q_z^0+G_z)]z}}{b_\parallel^2+[-i(q_z^0+G_z)]^2}\left\{\big[-i\big(q_z^0+G_z\big)\big]\cos(b_\parallel z)+b_\parallel\sin(b_\parallel z)\right\}\right|_{d_v}^{0}\right\}\end{aligned}\tag{55}$$

The quantity $\varepsilon^{-1}_{\text{slab}}(\mathbf{q}_\parallel+\mathbf{G}_\parallel,q_z^0+G_z,q_z^0+G'_z,\omega)$ is a function of the loss energy ω and the transferred momentum $\mathbf{q}_\parallel$, which is itself a smooth function of ω, being solely determined by the kinematic conditions:

$$|\mathbf{q}_\parallel|=\sqrt{2E_0}\sin(\theta_0)-\sqrt{2(E_0-\hbar\omega)}\sin(\theta_0+\psi)\tag{56}$$

In practical *ab initio* calculations, however, $\varepsilon^{-1}_{\text{slab}}(\mathbf{q}_\parallel+\mathbf{G}_\parallel,q_z^0+G_z,q_z^0+G'_z,\omega)$ is generally computed over a *finite* mesh of **k**-points, and this mesh subsequently determines the set of available $\{\mathbf{q}_\parallel\}$ values. In our implementation of this theory in the Yambo [32] code, we interpolate the dielectric matrices as a function of $\hbar\omega$ between each allowed $\mathbf{q}_\parallel(\hbar\omega)$ value, thus obtaining a continuous loss spectrum for all energies: using a sufficiently dense mesh of **k**-points ensures that this procedure does not introduce significant errors.

6.3. Practical example

We now present a illustrative example of the above derived theory, and compare it with the corresponding result obtained within the three-layer model. The system examined is the GaAs(001)–$c(4\times4)$ surface which allows a good test of the two models since high resolution experimental spectra are available for $\mathbf{q}_\parallel$ aligned explicitly along high symmetry directions of the surface, that is, parallel and perpendicular to the dimer rows [3]. Therefore, comparison can be made with the HREELS signal *anisotropy*, which has the advantage that some experimental unknowns cancel each other out. GaAs(001)–$c(4\times4)$ is known [28] to exist in (at least) two distinct surface geometries: a symmetric dimer geometry, featuring three As–As dimers per unit cell, and a mixed dimer geometry, featuring Ga–As heterodimers (see Fig. 5). Results were obtained within DFT–RPA: further details of the calculations can be found in [15].

From the figure it is clear that the three-layer scheme already provides a reasonable description of the energy loss experiment, as the calculation succeeds in reproducing the anisotropy peak observed around 2 eV. It is also capable of differentiating between the two surface reconstructions, thus confirming that the mixed dimer model is that observed in the experiment. The results support the use of optical dielectric functions in Eq. (43), even though here $\mathbf{q}_\parallel$ is fairly large (of the order of 0.2 Å^{-1}).

HREELS spectra computed using the extended model are shown on the right of Fig. 5. We can draw a number of conclusions from the presented data. First of all, the general agreement with experiment is maintained. This is an important *a posteriori* validation of the application of the three-layer model to such calculations. Secondly, the new calculations actually improve upon the prior results. For instance, the negative peak at 2.9 eV is now reproduced at the correct energy, and the fine structure of the 2.0 eV peak is improved. This illustrates the importance of including the proper spatial and momentum behavior in $\varepsilon^{-1}_{\text{S.I}}(\mathbf{q}_\parallel,z,z',\omega)$. In the three-layer model, all the spatial information about the surface is averaged into a single function ε_s, which may not always be an adequate approximation.[2]

[2] The fact that the calculations continue to deviate from the experiment above 3.2 eV may indicate that other phenomena, outside the scope of our simulation, give rise to the loss signal above this energy.

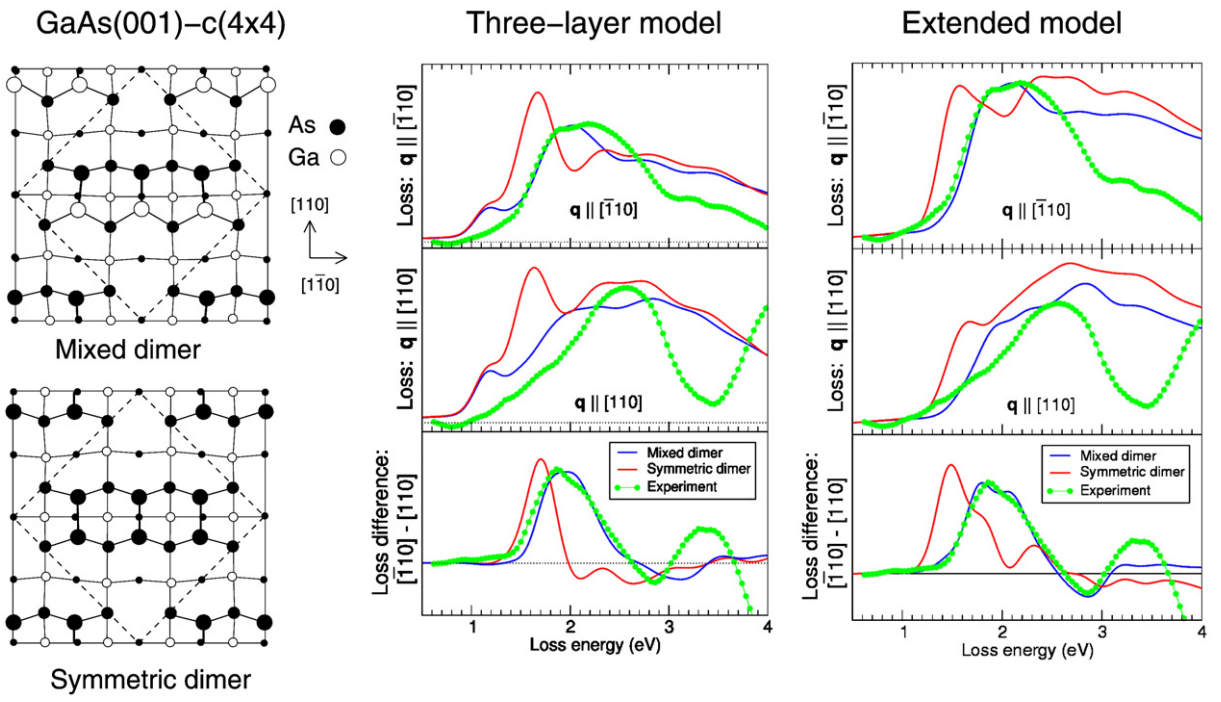

Fig. 5. HREELS spectra of the GaAs(001)–$c(4 \times 4)$ surface, computed within the anisotropic three-layer model (center) and the extended model described in the text (right). Experimental data is taken from [3] ($E_0 = 15$ eV; $\theta_0 = 45°$; $\psi = 0°$). Within each set of spectra, the top and middle panel show loss spectra for $\mathbf{q}_\parallel$ oriented parallel and perpendicular to the surface dimers, while the bottom panel shows the HREELS anisotropy signal. Two surface reconstructions are considered, as illustrated on the left-hand side.

Although the above calculations illustrate the use of the new theory as well as providing support for the three-layer model in computing HREELS spectra, the theory offers the potential for more interesting applications, for instance, computation of the wavevector dependence of the surface plasmon dispersion. Such calculations have mostly been carried out within models of the dielectric response [34], and *ab initio* calculations remain scarce (a notable exception being Silkin et al. [24]).

7. Final remarks

We have described a three-layer model for reflection EEL spectroscopy. The model can include many-body effects in the surface and bulk dielectric functions, as we have shown for the case of C(100). We have also outlined a more detailed theory, which avoids the three-layer approximation, and in some respects improves upon it. In particular, the depth of the surface layer may be a function of the energy loss, which is not described at all within the three-layer model. It is instead naturally embodied in the extended theory. In addition, the actual shape of the surface inhomogeneity, rather than a two-step model, is naturally included. Hence, local field effects perpendicular to the surface are fully described in the model. Important differences with respect to the three-layer model are expected to occur for large momentum transfers.

References

[1] H. Lüth, Surfaces and Interfaces of Solid Materials, Springer Study Edition, Berlin, Heidelberg, New York, 1995.
[2] H. Ibach, Phys. Rev. Lett. 24 (1970) 1416;
H. Ibach, Phys. Rev. Lett. 27 (1971) 253.
[3] A. Balzarotti, M. Fanfoni, F. Patella, F. Arciprete, E. Placidi, G. Onida, R. Del Sole, Surf. Sci. 524 (2003) L71–L76.
[4] F. Arciprete, C. Goletti, E. Placidi, P. Chiaradia, M. Fanfoni, F. Patella, C. Hogan, A. Balzarotti, Phys. Rev. B 68 (2003) 125328.
[5] W. Ho, R.F. Willis, E.W. Plummer, Phys. Rev. Lett. 40 (1978) 1463.
[6] S.Y. Tong, C.H. Li, D.L. Mills, Phys. Rev. Lett. 44 (1980) 407, and references therein.

[7] P.A. Thiry, M. Liehr, J.J. Pireaux, R. Caudano, Phys. Scr. 35 (1987) 368, and references therein.
[8] A.A. Lucas, M. Šunjić, Phys. Rev. Lett. 26 (1971) 229.
[9] D.L. Mills, Surf. Sci. 48 (1975) 59.
[10] H. Froitzheim, H. Ibach, D.L. Mills, Phys. Rev. B 11 (1975) 4980–4988.
[11] H. Ibach, D.L. Mills, Electron Energy Loss Spectroscopy and Surface Vibrations, Academic, 1982.
[12] A. Selloni, R. Del Sole, Surf. Sci. 186 (1986) 35.
[13] R. Esquivel-Sirvent, C. Noguez, Phys. Rev. B 58 (1998) 7367–7372.
[14] M. Palummo, O. Pulci, A. Marini, L. Reining, R. Del Sole, Phys. Rev. B 74 (2006) 235431.
[15] E. Placidi, C. Hogan, F. Arciprete, M. Fanfoni, F. Patella, R. Del Sole, A. Balzarotti, Phys. Rev. B 73 (2006) 205345.
[16] M. Kociak, O. Stéphan, L. Henrard, V. Charbois, A. Rothschild, R. Tenne, C. Colliex, Phys. Rev. Lett. 87 (2001) 075501.
[17] J.D.E. McIntyre, D.E. Aspnes, Surf. Sci. 24 (1971) 417.
[18] A. Cricenti, S. Selci, F. Ciccacci, A.C. Felici, C. Goletti, Z. Yong, G. Chiarotti, Phys. Scr. 38 (1988) 199–203.
[19] H. Ehrenreich, in: Proceedings of the International School of Physics "E. Fermi", corso XXXIV.
[20] G. Onida, L. Reining, A. Rubio, Rev. Mod. Phys. 74 (2002) 601, and references therein.
[21] R. Del Sole, E. Fiorino, Phys. Rev. B 29 (1984) 4631–4645.
[22] W. Hanke, L.J. Sham, Phys. Rev. Lett. 33 (1974) 582–585;
W. Hanke, L.J. Sham, Phys. Rev. B 12 (1975) 4501–4511.
[23] W. Hanke, Adv. Phys. 27 (1978) 287.
[24] V.M. Silkin, E.V. Chulkov, P.M. Echenique, Phys. Rev. Lett. 93 (2004) 176801.
[25] V. Olevano, L. Reining, Phys. Rev. Lett. 86 (2001) 5962–5965.
[26] H.H. Farrell, F. Stucki, J. Anderson, D.J. Frankel, G.J. Lapeyre, M. Levinson, Phys. Rev. B 30 (1984) 721.
[27] H. Ibach, J.E. Rowe, Phys. Rev. B 9 (1974) 1951–1957.
[28] A. Ohtake, J. Nakamura, S. Tsukamoto, N. Koguchi, A. Natori, Phys. Rev. Lett. 89 (2002) 206102;
C. Hogan, E. Placidi, R. Del Sole, Phys. Rev. B 71 (2005) R041308.
[29] S. Albrecht, L. Reining, R. Del Sole, G. Onida, Phys. Rev. Lett. 80 (1998) 4510–4513.
[30] T.W. Mercer, P.E. Pehrsson, Surf. Sci. 399 (1998) L327–L331.
[31] S. Botti, N. Vast, L. Reining, V. Olevano, L.C. Andreani, Phys. Rev. Lett. 89 (2002) 216803.
[32] A. Marini, C. Hogan, D. Varsano, M. Grüning, `yambo`: An *ab initio* tool for excited state calculations, Computer Physics Communications (2009), doi:10.1016/j.cpc.2009.02.003. See also http://www.yambo-code.org.
[33] See http://www.bethe-salpeter.org/.
[34] P.J. Feibelman, Phys. Rev. B 40 (1989) 2752–2756.